JOURNAL OF GEOPHYSICAL RESEARCH, VOL. 112, XXXXXX, doi:10.1029/2007JA012464, 2007

Simulations of Alfvén waves in the geomagnetic tail and their auroral signatures

Andrew N. Wright[1] and W. Allan[2]

Received 10 April 2007; revised 22 August 2007; accepted 3 October 2007; published XX Month 2007.

[1] Observations show that Ultra-Low Frequency (ULF) Alfvén waves in the magnetotail have distinctive properties depending upon their location. In particular, those in the plasma sheet boundary layer (PSBL) have a larger amplitude and favor earthward propagation compared to those in the tail lobe which have the polarization of standing waves. The PSBL waves are also associated with electron acceleration and optical auroral emissions that exhibit equatorward motion. In this paper we present simulations of MHD wave coupling in the magnetotail to support an explanation for how Alfvén waves with these properties may be established. The simulations also suggest the waves should have periods from 5 min to >20 min, and produce auroral emissions in the ionosphere having a latitudinal range of 40–130 km and equatorward speed of order 1 kms^{-1}. Field aligned currents are typically a few μAm^{-2}.

Citation: Wright, A. N., and W. Allan (2007), Simulations of Alfvén waves in the geomagnetic tail and their auroral signatures, *J. Geophys. Res.*, *112*, XXXXXX, doi:10.1029/2007JA012464.

1. Introduction

[2] Four decades ago it was realized that the Earth supported an extended magnetic tail. Early theoretical studies of this structure by *McClay and Radoski* [1967] and *Patel* [1968] showed that magnetohydrodynamic (MHD) normal modes of the tail have natural frequencies of the order of (or less than) millihertz, in agreement with magnetometer data [e.g., *Herron*, 1967]. The study of decoupled fast modes in more realistic tail equilibria has continued to receive attention [e.g., *Hopcraft and Smith*, 1986; *Edwin et al.*, 1986]. Subsequently the coupling of fast and Alfvén waves in the magnetotail has been of interest [see *Liu et al.*, 1995; *Allan and Wright*, 1998, 2000; *Wright et al.*, 1999] and has been reviewed by *Wright and Mann* [2007].

[3] Observations have provided considerable motivation for the above studies. In particular, optical auroral brightenings at the foot points of field lines carrying Alfvén waves have shown a common frequency [*Samson et al.*, 1996; *Xu et al.*, 1993] with the Alfvén wavefields. This indicates that the electrons carrying the field-aligned Alfvén wave currents are energetic enough to produce auroral enhancements when they precipitate during the upward current phase of the wave cycle. The study of electron dynamics in Alfvén waves is a topic of great interest. For example, *Dombeck et al.* [2005] show how the Poynting vector decreases with altitude between POLAR and FAST, and is associated with an increased electron energy flux. Similarly *Vaivads et al.* [2003] show the Poynting vector observed by Cluster when mapped earthward to DMSP is comparable to the electron energy flux there. These observations indicate that the energy required to accelerate electrons to carry the Alfvén wavefield aligned current can be a significant sink of wave energy. Indeed *Wright et al.* [2003] showed this loss mechanism could exceed the traditional damping process associated with Ohmic heating in the ionosphere.

[4] The optical auroral features associated with Alfvénic electron precipitation will share the same latitudinal phase motion as the Alfvén wave. Observations by *Liu et al.* [1995] and *Wright et al.* [1999] show equatorward phase motion suggesting the waves are on field lines threading the plasma sheet boundary layer (PSBL). It is possible that these waves can account for the Poleward Boundary Intensifications (PBIs) reported by *Lyons et al.* [2002] (located on the poleward edge of the auroral oval, and thought to map to the PSBL), which are associated with activity in the tail.

[5] The most recent observations in this area are in situ measurements of wavefields in the magnetotail [e.g., *Keiling et al.*, 2005]: Lobe Alfvén waves are shown to be excited by substorms and can have a standing wave structure, even on open field lines, while PSBL Alfvén waves have a larger amplitude than those in the lobe. [*Wygant et al.*, 2000; *Keiling et al.*, 2005] correlate earthward Poynting vector with auroral luminosity, and hence the energy of precipitating electrons, which it is sufficient to supply. Interestingly, the PSBL waves appear to be composed of an earthward propagating wave plus a partially reflected (anti-earthward) wave. The latter is sometimes negligible, and ultra-low-frequency (ULF) PSBL waves show a bias toward being earthward propagating and having an earthward directed Poynting vector [*Wygant et al.*, 2000; *Keiling et al.*, 2002, 2005].

[1]Mathematical Institute, University of St. Andrews, St. Andrews, Fife, UK.
[2]National Institute of Water and Atmospheric Research, Wellington, New Zealand.

0148-0227/07/2007JA012464$09.00

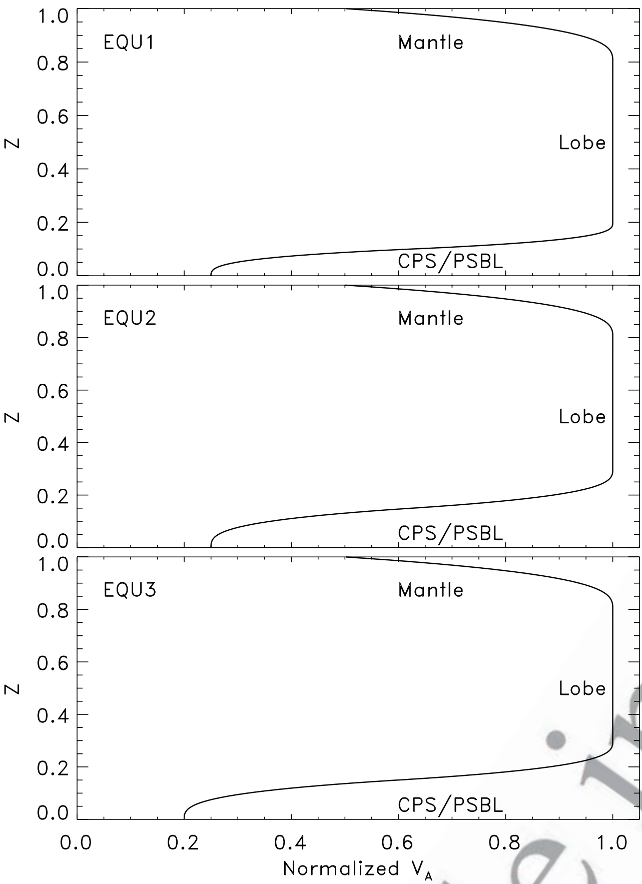

Figure 1. The variation of Alfvén speed with z across the northern half of the tail. Length is normalized by the tail half-width, with z = 0 being at the center of the plasma sheet.

[6] In this paper we apply an adaptation of the model developed by *Allan and Wright* [2000]. We focus on the parametric dependence of PSBL and lobe Alfvén waves on the cross-tail wave number, and develop a scenario consistent with the following observations:

[7] (1) The Alfvén wave amplitude in the PSBL exceeds that in the lobe.

[8] (2) The lobe Alfvén waves have a standing structure, while those in the PSBL are earthward propagating.

[9] (3) The PSBL waves produce optical auroral emissions, while those in the lobe do not.

[10] (4) The periods of PBI features ranges from 5 min to >20 min.

[11] (5) PBIs have a latitudinal extent of 40-130 km and have an equatorward motion of 0.2–0.7 km s^{-1}.

[12] (6) Field aligned currents in the ionosphere can reach several μAm^{-2}.

2. Model

2.1. Equilibrium

[13] We model the equilibrium magnetotail as a simple waveguide with the structure described in detail in section 2 of *Allan and Wright* [2000]. We normalize all Alfven speeds in the model to the lobe Alfven speed V_{AL} and lengths by the tail half-width z_M. We employ three equilibria in this paper, all having V_2 = 1.0, V_3 = 0.5 and z_2 = 0.8. Other parameters are:

$$\mathrm{EQU1}: \mathrm{V_1} = 0.25, \mathrm{z_1} = 0.2$$
$$\mathrm{EQU2}: \mathrm{V_1} = 0.25, \mathrm{z_1} = 0.3$$
$$\mathrm{EQU3}: \mathrm{V_1} = 0.20, \mathrm{z_1} = 0.3$$

[14] Here V_1, V_2 and V_3 are Alfvén speeds respectively at the magnetotail central plane (z = 0), in the magnetotail lobe, and at the magnetopause (z = 1). The lobe lies between z_1 and z_2. Figure 1 displays the variation of V_A with z for these three equilibria.

[15] Of course, the magnetotail is not a cold plasma, as our model assumes, and β is certainly greater than 1 in the plasma sheet. However, the fast mode propagates at a speed $c_f = \sqrt{V_A^2 + c_s^2}$ (where c_s is the sound speed) which is surprisingly insensitive to the details of how our equilibrium satisfies total pressure balance across the tail. For example, *Allan and Wright* [2000] show that the fast speed differs by less than 10% in the two extreme cases of a cold plasma sheet and a field-free plasma sheet. Consequently our equilibrium should give a good representation of fast mode propagation.

2.2. Governing Equations

[16] As mentioned previously, length is normalized to the tail half-width (in z), z_M, and velocity by the maximum Alfvén speed in the lobe, V_{AL}. Thus the normalizing time unit is z_M/V_{AL}. Magnetic fields are normalized by the equilibrium field strength, B_0, and hence densities by $B_0^2/\mu_0 V_{AL}^2$. The normalized linear cold plasma ideal MHD equations for the perturbed magnetic field, **b** = (b_x, b_y, b_z), and velocity, **u** = (0, u_y, u_z) are

$$\partial b_x/\partial t = -\left(\partial u_z/\partial z + k_y u_y\right) \quad (1)$$

$$\partial b_y/\partial t = \partial u_y/\partial x \quad (2)$$

$$\partial b_z/\partial t = \partial u_z/\partial x \quad (3)$$

$$\partial u_y/\partial t = \left(\partial b_y/\partial x + k_y b_x\right)/\rho \quad (4)$$

$$\partial u_z/\partial t = (\partial b_z/\partial x - \partial b_x/\partial z)/\rho. \quad (5)$$

[17] The velocity component u_y is chosen to have a separable y-dependence of sin($k_y y$), and other perturbations have a sin($k_y y$) or cos($k_y y$) dependence consistent with this. The above equations then give the evolution of **b**(x, z, t) and **u**(x, z, t). Details of the numerical method used to solve (1)–(5) are given by *Allan and Wright* [2000].

2.2.1. Boundary Conditions

[18] The boundary conditions we apply are the same as that by *Allan and Wright* [2000], except as described in the following. The earthward end of the simulation domain (in normalized units) is located at x = x_M. One boundary

condition we adopt here corresponds to a perfectly reflecting ionosphere. This is implemented by having the ionosphere (which is located at $x = x_I$) coincide with the earthward end of the domain (i.e., $x_I = x_M$), and apply perfect reflection of waves there consistent with $u_z = 0$. The other ionospheric boundary condition we employ is a perfectly absorbing ionosphere, and corresponds to an "outgoing wave" condition at the ionosphere (x_I), with no reflected waves. This is achieved by simply extending the simulation domain beyond the ionosphere (i.e., $x_M > x_I$). The region corresponding to the magnetotail is $0 < x < x_I$, and the region $x_I < x < x_M$ is a buffer zone into which waves reaching the ionosphere can propagate. We set x_M to be sufficiently large that any waves reaching x_M will not have time to return to x_I. Hence the region $0 < x < x_I$ (the magnetotail) will appear to allow waves to propagate up to and through the boundary at x_I as if being perfectly absorbed there. Also note that our equilibrium does not allow for the converging field geometry as the ionosphere is approached. We discuss how the wavefields will be modified by this feature in section 4.

[19] The tailward boundary of the simulation domain (at $x = 0$) employs the symmetry condition $\partial u_z/\partial x = 0$. Other wavefields at the boundaries have nodes/antinodes as required for consistency with the equations (1)–(5).

[20] For computational efficiency we solve only in the space $z \geq 0$, and the boundary condition at $z = 0$ is chosen to represent either even modes (in z) of the waveguide ($u_z = 0$) or odd modes ($b_x = 0$). These conditions are applied along the x axis at all times except over $0 < x < x_d$ during the "driving" phase, $0 < t < t_d$, when either u_z (even) or b_x (odd) is proportional to

$$\cos(\pi t/t_d)[1 - \cos(2\pi t/t_d)]^2[1 + \cos(\pi x/x_d)]. \qquad (6)$$

[21] Other variables are updated on $z = 0$ according to (1)–(5) using one-sided derivatives in z when required. (The details of this method of driving were developed by *Wright and Rickard* [1995].) Numerical results are normalized by having the maximum value of $u_z(x = 0, z = 0, 0 < t < t_d)$ equal to unity. *Allan and Wright* [2000] explain how x_d and t_d can be chosen to represent the effect of a plasmoid forming and being ejected. In the even mode simulation the plasmoid is perfectly symmetric about $z = 0$. If there is some asymmetry odd modes will also be present. The general case is a superposition of both even and odd modes.

2.2.2. Numerical Accuracy

[22] The wavefields that evolve tend to have a small spatial scale in z where dV_A/dz is largest, and can reduce as time increases due to phase mixing [e.g., *Allan and Wright*, 2000]. It is important to ensure that this scale is properly resolved by the grid. The results in this paper have either $\Delta z = 2.5 \times 10^{-4}$ or $\Delta z = 5 \times 10^{-4}$. The time step is then determined by the CFL condition and Δz. We used $\Delta t = 10^{-4}$ and $\Delta t = 2 \times 10^{-4}$, respectively for the two Δz resolutions. The waves do not have a particularly small scale in the x direction, and Δx was taken as 2×10^{-2}.

[23] To check numerical convergence we compared the u_z fields calculated with the above resolution against a simulation using double the resolution in space and time [see *Allan and Wright*, 2000]. For the results presented here the fields had converged to better than 0.05%. We also compared the Poynting flux energy flow in to the domain across the boundary during driving to the volume integrated energy density at the end of the simulation. This showed our ideal simulations conserved energy well as their ratio was at least 0.99995. Preservation of $\nabla \cdot \mathbf{b} = 0$ was checked, and reached a maximum value of 10^{-11} throughout the simulations, being limited by machine precision.

3. Magnetotail Alfvén Waves

3.1. Previous Studies

[24] Considerable theoretical work has been carried out on the coupling of different MHD waves in nonuniform media. The basis of our understanding of ULF Alfvén waves on closed field lines comes from normal modes ($\propto \exp[-i\omega t]$) of a 1D equilibrium where the wavefields have a single field-aligned wave number ($k_\|$), and perpendicular wave number (k_y). The equilibrium is nonuniform in the third direction, and the wavefields are governed by an ordinary differential equation in this coordinate [e.g., *Southwood*, 1974; *Chen and Hasegawa*, 1974].

[25] These studies give much insight into the behavior of wave coupling on closed field lines, where the presence of the ionosphere determines the value of $k_\|$. They show that on field lines where $\omega_A (= k_\| V_A)$ is equal to ω (which may be regarded as the fast mode driving frequency), efficient coupling leads to the Alfvén mode absorbing energy from the fast mode. Moreover, these modes decouple when $k_y = 0$ or $k_y \rightarrow \infty$, and an optimum k_y for maximum efficiency can be identified [e.g., *Kivelson and Southwood*, 1986]. Coupling also depends upon the Alfvén speed gradient: Let us suppose the Alfvén speed changes by ΔV_A over a length scale ℓ. In the limit $\ell \rightarrow \infty$ the gradient of V_A tends to zero, the medium becomes uniform and the waves decouple. Similarly, in the limit $\ell \rightarrow 0$ the gradient becomes infinite. Now the equilibrium appears to have a jump in V_A, and again no wave coupling occurs. (In this limit the coupling strength is inversely proportional to the Alfvén speed gradient [e.g., *Ruderman and Roberts*, 2002].) For intermediate gradients wave coupling does occur. The properties described above give considerable insight into wave coupling, even when the prescription of $\exp[-i\omega t]$ is relaxed. For example, the time-dependent studies of *Allan et al.* [1986] and *Mann et al.* [1995] show the location of wave coupling is still accurately predicted by normal mode ideas, but that the concept of phasemixing is now required. Other studies have considered time-dependent coupling in a dipole geometry [*Lee and Lysak*, 1989] and shown the persistence of wave coupling. Most recently the standing nature of waves along $\mathbf{B}$ has been relaxed [*Allan and Wright*, 2000, and references therein]. These studies solve for the wavefields as functions of the field-aligned coordinate and time. (Only k_y is imposed.) Wave coupling still occurs in such a system, as does phasemixing. However, the variation along $\mathbf{B}$ is completely different to that on closed field lines, and the possibility of singularities and infinite Alfvén wave amplitudes that existed in earlier driven studies does not exist in this case. Indeed, although early studies can give some qualitative understanding of some of the features seen in wave coupling on open field lines, the closed field line theory cannot, for example, quantify the amplitude of the Alfvén waves excited in our simulation.

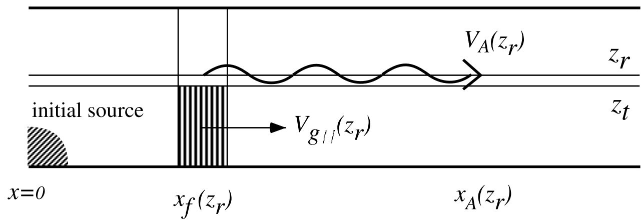

Figure 2. A source of fast modes waves exists at the center of the plasma sheet, and may be viewed as a set of wave packets. The behavior of one particular wave packet is shown: It has a turning point at z_t and propagates earthward with a group velocity $V_{g\|}$. A little beyond z_t (at z_r) its parallel phase speed matches that of Alfvén waves, and mode coupling occurs. The Alfvén wave travels earthward at speed $V_A(z)$ ($>V_{g\|}$), and so runs ahead of the fast wave packet. (The Earth is to the right of this figure.)

3.2. Waveguide Mode Coupling

[26] The driving conditions described in section 2.2.1 introduce primarily fast mode disturbances into the tail. If $k_y = 0$ the energy remains in the fast mode while dispersing and propagating along the tail waveguide. In this case there is no coupling to Alfvén waves, which are characterized by the u_y and b_y fields. When $k_y \neq 0$ the fast mode waves will couple to Alfvén waves as shown in Figure 2: The source of waves centered on $(x, z) = (0, 0)$ can be thought of as a superposition of fast mode wave packets, described via the fast mode dispersion relation $\omega_n(k_\|)$. Here $k_\| \equiv k_x$, the field-aligned wave number, and k_y has some chosen (fixed) value. The subscript n refers to the harmonic number in z. On field lines where the Alfvén speed ($V_A(z)$) is equal to the field-aligned fast mode phase speed ($\omega_n(k_\|)/k_\|$) efficient mode conversion to the Alfvén mode may take place, driving an Alfvén wave of frequency $\omega_A(z) = \omega_n(k_\|)$ and wave number $k_{\|A}(z) = k_\|$. This much is familiar from early studies of wave coupling on closed field lines [e.g., *Southwood*, 1974; *Chen and Hasegawa*, 1974]. Consideration of a different $k_\|$ identifies a different phase speed ($\omega_n(k_\|)/k_\|$) and hence a different field line where $V_A(z)$ is matched. Thus both ω_A and $k_\|$ will vary across the PSBL and lobe. This is very different to early studies where $k_\|$ could not vary continuously. Our (open field line) model admits a continuum of $k_\|$, and hence has a layer of "resonant" field lines, rather than a discrete (singular) resonant field line.

[27] The Alfvén waves in our simulations run along the field line at a speed $V_A(z)$, while the fast mode wave packet driving these waves travels along the guide at a slower speed $V_{g\|}(k_\|) = \partial\omega_n(k_\|)/\partial k_\|$ (see *Wright et al.* [1999] and *Wright and Mann* [2007] for more details).

[28] *Allan and Wright* [1998] presented the first study of coupled waves in the magnetotail waveguide. To facilitate the interpretation of their simulation results, they adopted a small value for k_y of 0.5, which is the weak coupling limit. This permitted the use of decoupled ($k_y = 0$) modes and dispersion relations as an approximation for the weakly coupled modes, and allowed for a clear identification of the physics operating. Subsequently, *Allan and Wright* [2000] attempted a realistic study of waves in the tail by adopting a realistic $V_A(z)$ profile and taking $k_y = 1.3$, which corresponds to the fundamental mode from dawn to dusk. For EQU1 ("Model A" in their study) and driving u_z with parameters $t_d = 1.0$ and $x_d = 0.48$, Figure 3a shows contours of the Alfvén wave amplitude (when $k_y = 1.3$ and $t = 6.0$) through the quantity $\sqrt{E_A}$, where the Alfvén wave energy density is

$$E_A = \frac{1}{2}\left(\rho u_y^2 + b_y^2\right), \tag{7}$$

and is adapted from their Figure 4. Notice how the PSBL Alfvén waves (centered on $z = 0.125$) have a strong phase mixing gradient which leads to substantial field aligned currents ($j_\|$). In contrast the lobe ($0.2 < z < 0.8$) has

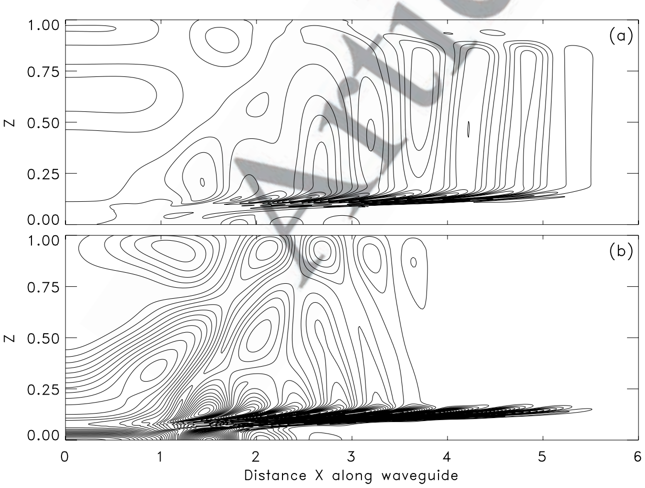

Figure 3. The variation of Alfvén wave amplitude with x and z at $t = 6.0$. Only the northern half of the tail is shown. The wave source was centered on (0, 0), and energy propagates earthward to $x > 0$. The dawn-dusk wave number, k_y, is taken to be 1.3 in panel (a) and 7.5 in panel (b). The PSBL ($0.1 < z < 0.2$) and lobe ($0.2 < z < 0.8$) both carry Alfvén waves with similar amplitude in Figure 3a, while in Figure 3b those in the PSBL are far larger than those in the lobe. [Model used is EQU1 with $t_d = 1.0$, $x_d = 0.48$, $t = 6.0$.]

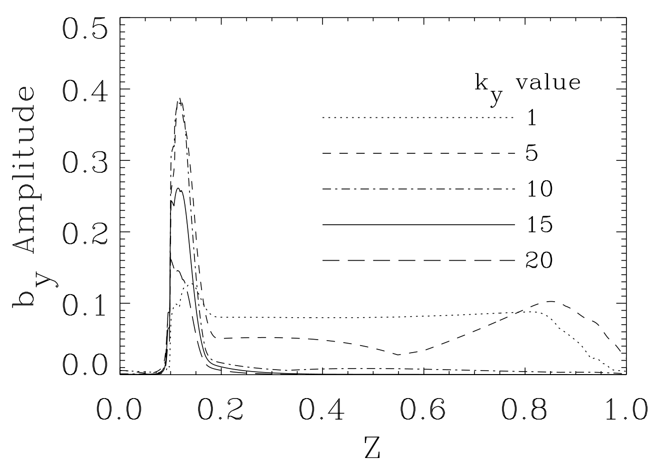

Figure 4. The variation of Alfvén wave b_y amplitude across the tail for different k_y. The PSBL is centered on $z = 0.125$.

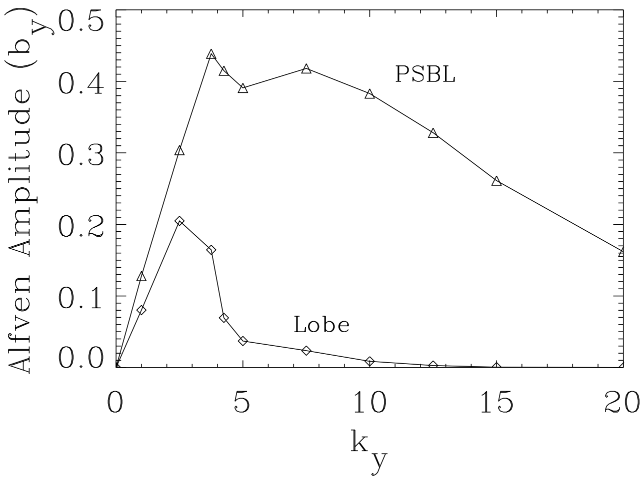

Figure 5. Comparison of Alfvén wave b_y amplitude in the PSBL and in the lobe as a function of k_y.

essentially a plane propagating Alfvén wave over $3 < x < 6$ and little phase mixing or $j_{\|}$.

[29] While these results may agree with many features in observations, they do not account for the recent bias reported by *Wygant et al.* [2000] and *Keiling et al.* [2002] for the Alfvén wave b_y to be greater in the PSBL than in the lobe. In an effort to address this we present new results in Figure 3b. These have the same parameters as the simulation in Figure 3a except k_y was increased from 1.3 to 7.5. The contour values in the two panels are the same, and it is evident that the Alfvén wave amplitude in the PSBL far exceeds that in the lobe over $3 < x < 6$.

[30] To investigate the wave amplitude dependence on k_y we performed simulations for several values of k_y. For each run the final snapshot at $t = 6.0$ was examined as follows: For a given z the "Alfvénic" region was identified (typically $3 < x < 6$) and the maximum amplitude of b_y logged. This procedure was repeated for all z, and the results are displayed in Figure 4. It is clear that for all but the smallest k_y there is stronger coupling to Alfvén waves in the PSBL (centered on $z = 0.125$) than in the lobe ($0.2 < z < 0.8$). The presence of the largest Alfvén wavefields in the PSBL is consistent with the dependence of coupling strength on Alfvén speed gradient. Evidently the PSBL provides the optimum condition of a moderate gradient. Figure 5 summarizes this behavior by taking $b_y(z = 0.125)$ and $b_y(z = 0.5)$ to represent the wave amplitude in the PSBL and lobe, respectively, and showing their variation with k_y. For a large range of k_y(>5) the PSBL amplitude exceeds that in the lobe by an order of magnitude or more. The dependence of coupling strength on wave number is familiar from the related, but different, studies in a box model applicable to closed field lines [e.g., *Kivelson and Southwood*, 1986].

4. Field-Aligned Currents and Auroral Signatures

[31] Observations show that the large Poynting vector in the PSBL is correlated with auroral intensity [*Wygant et al.*, 2000; *Keiling et al.*, 2002] and hence energy of precipitating electrons. Auroral enhancements on the poleward edge of the auroral oval are thought to map to the PSBL and show repetitive equatorwards motion [*Wright et al.*, 1999; *Lyons et al.*, 2002] which is consistent with the phase motion of PSBL waves in simulations [*Liu et al.*, 1995; *Allan and Wright*, 1998, 2000]. Observations suggest that much of the earthward Poynting flux can be converted to precipitating electron energy flux [*Wygant et al.*, 2000], which could lead to a significant loss of wave energy [*Wright et al.*, 2003] and an absence of a reflected wave from the ionosphere.

[32] Standing Alfvén waves on closed field lines have been shown to produce periodic enhancements in auroral optical emissions with the same period as the Alfvén wavefields [*Samson et al.*, 1996; *Xu et al.*, 1993]. *Lotko et al.* [1998] reported how FAST (at ~4,000 km altitude) observed Alfvén wavefield-aligned currents of several μAm^{-2} to be carried by electrons moving with keV energies. Subsequently, *Samson et al.* [2003] showed how meridian scanning photometer (MSP) and ground magnetometer data for this event were associated with a standing Alfvén wave on closed field lines. In particular, the motion of arcs was poleward, whereas propagating Alfvén waves in the PSBL generally produce equatorward motion [e.g., *Allan and Wright*, 2000].

[33] The first step in relating our simulations to the above observations is to chose a normalization and calculate the field aligned current in the magnetotail. To obtain realistic quantities from our simulations we begin by adopting the following normalization: B_0 = 10 nT; V_{AL} = 700 kms^{-1} (lobe Alfvén speed); z_M = 25 R_E (tail half-width). These give our time unit as 227.5 s (about 4 min). *Allan and Wright* [1998, 2000] suggest the driving parameters we adopt are representative of space and timescales associated with plasmoid ejection, when the amplitude of $u_z(0, 0, 0 < t < t_d)$ is $\approx$320 kms^{-1}.

[34] The cross-tail (dawn-dusk) scale of the waves, when $k_y = 1.3$, gives a half wavelength of 60 R_E and corresponds to the fundamental mode in y. This was the value of k_y used by *Allan and Wright* [2000] and Figure 3a. The strong coupling case of $k_y = 7.5$ employed in Figures 6 and 7 gives a half wavelength of 10 R_E, and it is likely that plasmoids or wave sources with this extent in y will produce fast modes that couple particularly efficiently to Alfvén waves in the PSBL.

4.1. Mapping Between the PSBL and Ionosphere

[35] The physics embedded in our straight magnetic field equilibrium will not describe how Alfvén waves propagate and evolve in the near-Earth dipole field geometry they encounter as the ionosphere is approached. Some insight into the effect of the nonuniform **B** can be gained by considering the extent to which a purely dipole field changes between the equatorial plane and the ionosphere. We can then use these properties to map waves from the tail down to the ionosphere. Using the definitions of the dipole field metric functions given, for example, by *Allan and Knox* [1979], the decrease in unit length between equatorial plane and ionosphere in the "radial" direction perpendicular to L shells is

$$Z_{sc} = 2L\sqrt{L - 0.75} \tag{8}$$

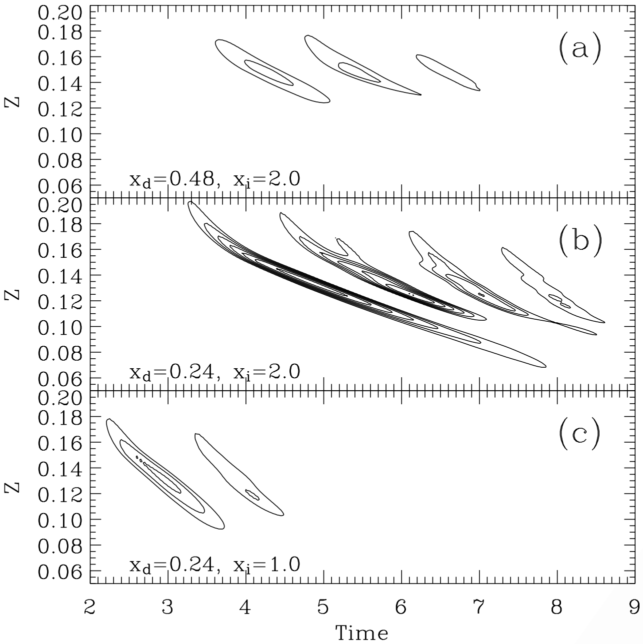

Figure 6. Upward field aligned current density at the ionospheric end using EQU2 with $t_d = 1.0$ and ($k_y = 7.5$) as a function of z and time. Other parameters are given in each panel. The region $0.1 < z < 0.2$ corresponds to the PSBL. The contours are chosen so that, when mapped to the ionosphere, they correspond to upward current densities of 0.5, 1.0, 1.5,...μAm^{-2}. The driver symmetry only excites modes that are antisymmetric in u_z about $z = 0$.

The corresponding scale factor in the azimuthal direction is

$$Y_{sc} = L^{3/2} \tag{9}$$

Therefore unit area in the equatorial plane decreases on mapping to the ionosphere by a factor

$$A_{sc} = Z_{sc} \times Y_{sc} = 2L^{5/2}\sqrt{L - 0.75} \tag{10}$$

The increase in current density between the equatorial plane and ionosphere is proportional to A_{sc}. If the outer limit of the PSBL is at $L = 8$, the value of A_{sc} is 975. If the outer limit is at $L = 12$, $A_{sc} = 3346$. These cover the range of L values quoted by *Keiling et al.* [2002] whose data we compare with later. Note that typical stretching of the tail magnetic field on the nightside implies that the dipole field A_{sc} values quoted are lower limits on the values, and hence current density enhancements, in a realistic magnetotail structure.

[36] Besides mapping $j_\parallel$ to the ionosphere we will want to translate scales in the z direction (measured in the tail) to latitudinal scales in the ionosphere. The simulation scales will need to be reduced by Z_{sc} to estimate the ionospheric scales. For an $L = 8$ field line this corresponds to a factor of 43.1, while that for an $L = 12$ field line is 80.5.

[37] To investigate the likely auroral signatures in optical data we choose the outgoing wave condition at the ionospheric boundary, since the main area of interest is the PSBL field lines. The field-aligned current is calculated from $\mu_0 j_\parallel = \partial b_z/\partial y - \partial b_y/\partial z$ at the notional ionospheric boundary. In the simulation, this boundary is simply the plane $x = x_I$ which we then map to give representative ionospheric fields. Within the normalization and mapping described earlier in this section we produce contour plots of upward ionospheric current density as these are likely to produce optical auroral emissions.

4.2. Even Modes

[38] Figure 6 shows simulations of even modes (i.e., ones for which u_z is antisymmetric about $z = 0$). The contours indicate upward ionospheric currents that would be expected to produce optical auroral emissions. The background model is EQU2 ($V_1 = 0.25$, $V_2 = 1.0$, $V_3 = 0.5$, $z_1 = 0.3$, $z_2 = 0.8$), the duration of the driver was $t_d = 1.0$, and the strong coupling limit ($k_y = 7.5$) is assumed. In Figure 6a the driving displacement (centered on $x = 0$) has an extent $x_d = 0.48$, and

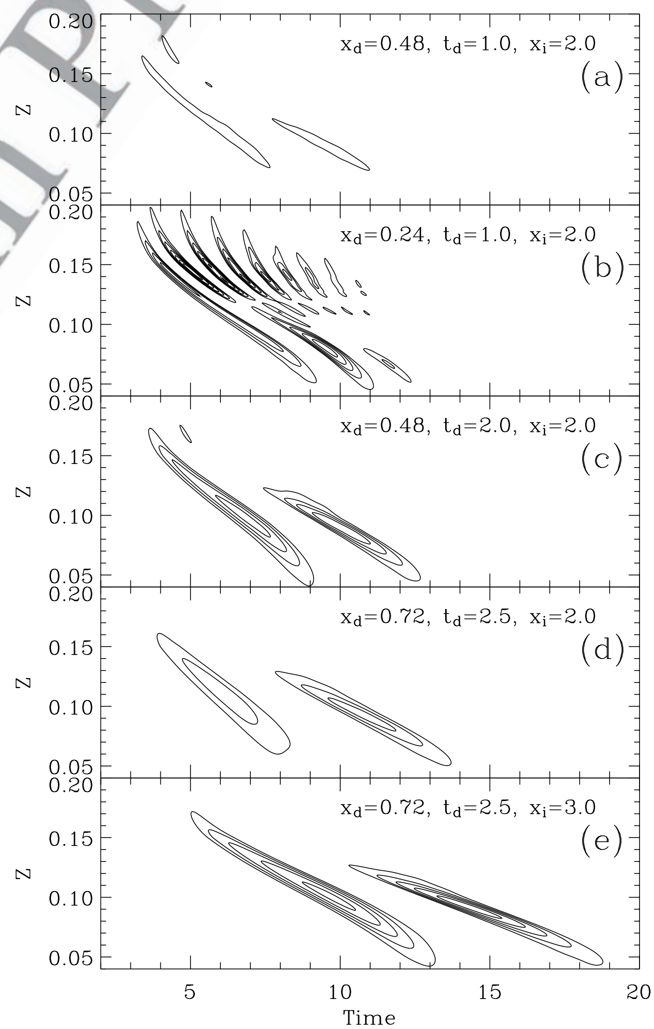

Figure 7. Upward field aligned current density at the ionospheric end using EQU3 with $k_y = 7.5$ as a function of z and time. Other parameters are given in each panel. The region $0.05 < z < 0.2$ corresponds to the PSBL. The contours are chosen so that, when mapped to the ionosphere, they correspond to upward current densities of 0.5, 1.0, 1.5,...μAm^{-2}. The driver symmetry only excites modes that are symmetric in u_z about $z = 0$.

the ionosphere is at $x_I = 2.0$. Three equatorward moving arcs are evident, associated with upward currents exceeding 1 μAm^{-2}.

[39] To explore the dependence of arc structure on our parameters, we changed the extent of the driver to $x_d = 0.24$ and show the results in Figure 6b. (All other parameters are as in (a).) The effect is to intensify the currents ($\sim$4 μAm^{-2}) and increase the latitudinal range of the arcs. The slope of the arcs gives the north-south phase speed which *Wright et al.* [1999] show is given by

$$V_{pz}(x,z,t) = \frac{-V_A(z)}{dV_A/dz} \cdot \frac{V_A(z) - V_{g\|}(z)}{x - V_{g\|}(z)t}. \qquad (11)$$

Here $V_{g\|}(z)$ is the parallel group velocity of the fast mode that couples to Alfvén waves on the field line at z.

[40] In Figure 6c we adopt the same parameters as in (b), except that the ionosphere is closer ($x_I = 1.0$, rather than 2.0). This results in an earlier arrival time of the waves at the ionosphere. We also note that the arcs in (c) have a greater phase velocity (steeper slope) than in (b). This can be understood using (11) to estimate the phase velocity at the leading edge of the Alfvén wave signal at a given z: If the waves here are propagating at speed $V_A(z)$, the leading edge will be located at $x = V_A(z)t$. Hence (11) gives

$$V_{pz}(x = V_A(z)t, z, t) = \frac{-V_A}{dV_A/dz} \cdot \frac{1}{t} \qquad (12)$$

and it is evident that the earlier the first arc appears, the larger its phase speed will be. This can also be understood physically: As the Alfvén waves propagate earthward they phasemix and develop structure in the z direction. The further they propagate, the smaller the scales in z (and larger k_z) becomes. Thus the phase speed ($V_{pz} = \omega_A(z)/k_z$) becomes reduced as x_I is increased.

4.3. Odd Modes

[41] The even fast modes of the tail that were considered in the previous subsection represent only half the normal modes. The other half are odd, and have an antinode of u_z at $z = 0$. The fundamental mode is odd and corresponds to a flapping motion of the tail in which the central plasma sheet is displaced from its equilibrium position.

[42] We investigate the behavior of the odd modes of the tail in equilibrium EQU3 ($V_1 = 0.2$, $V_2 = 1.0$, $V_3 = 0.5$, $z_1 = 0.3$, $z_2 = 0.8$) and retain $k_y = 7.5$ which still corresponds to efficient coupling to Alfvén waves.

[43] Figure 7 displays upward current density contours. In (a) the driver parameters are $x_d = 0.48$ and $t_d = 1.0$, while the ionosphere is at $x_I = 2.0$. Fairly weak currents are produced in the PSBL near where dV_A/dz has its maximum value ($z = 0.15$). If the driver is localized more ($x_d = 0.24$) the effect is to excite higher harmonics [as noted by *Allan and Wright*, 2000], and with a greater amplitude as seen in (b) leading to large $j_\|$($\sim$3.5 μAm^{-2}) using the conservative $A_s c$ value of 975 discussed in section 4.1. The shortest period signatures appear to be confined to the outer PSBL ($z \approx 0.15$).

[44] The effect of increasing the driver period from $t_d = 1.0$ (a) to $t_d = 2.0$ (c) is to increase the amplitude of $j_\|$($\sim$2 μAm^{-2}). The longer driving period also places more energy in the lower frequency fast modes, which couple to corresponding lower frequency Alfvén waves (found at lower z).

[45] In panel (d) we see the effect of increasing x_d to 0.72 and increasing t_d to 0.25 (compared to (a)) is to produce arcs of moderate current strength ($j_\| \sim 1.5\mu$Am^{-2}) without higher harmonics present. If these parameters are retained, but the ionosphere is moved from $x_I = 2.0$ to $x_I = 3.0$, the results in (e) are produced. Here we can clearly see how the increased propagation time allows for more phasemixing which results in a larger k_z, associated with smaller phase speeds and an enhanced $j_\|$($\sim$2.5μAm^{-2}).

4.4. Phasemixing, $j_{\|}$, Electron Flux and Wave Propagation

[46] It is evident from Figures 6 and 7 that the strongest current can be found in the PSBL ($0.05 < z < 0.2$). This is qualitatively in accord with ideas familiar from closed field line studies: The Alfvén waves are excited where there is a moderate variation of V_A, (e.g., Figure 4). Moreover $j_\|$ is enhanced by phasemixing of the Alfvénic fields, which will occur preferentially where V_A changes – i.e., in the PSBL. (It should be noted that there are differences in the details of phasemixing on open and closed field lines as $k_\|$ varies with field line in the former, rather than being fixed, as in the latter.)

[47] Our simulations suggest that $j_\|$ reaching the ionosphere will easily reach several μAm^{-2} on PSBL field lines, and be less than $\sim$1 μAm^{-2} on lobe field lines. Although our MHD simulations say nothing about electron energy, it is well established in observations that PSBL currents are carried by electrons with energies of several keV [e.g., *Lotko et al.*, 1998] which produce optical auroral emissions [*Samson et al.*, 2003]. Thus it is to be expected that the upward current density contours in Figures 6 and 7 will be a reasonable proxy for Meridian Scanning Photometer (MSP) auroral observations. A similar approach was adopted by *Samson et al.* [2003], except they considered standing Alfvén waves on closed field lines. *Liu et al.* [1995] considered open field lines (although with a unique $k_\|$) and produced current density plots that are qualitatively similar to those in our figures. They also linked the simulation field aligned current with arcs in MSP data. Note that the periodic dependence on the field aligned coordinate makes the calculation of Liu et al., formally identical to closed field line studies. In contrast, our simulation has a finite (not infinite) wave train along the field line, and this limits the number of arcs that can be produced.

[48] With the above considerations we may expect to see MSP data exhibit features similar to those in Figures 6 and 7 when covering PSBL field lines. The distinctive negative slope (equatorward motion) is familiar from data. Moreover, it is interesting to note from (11) that $V_{pz} \propto (dV_A/dz)^{-1}$, and this accounts for the increasing slope at the top of the PSBL ($z \approx 0.18$) seen clearly in the first arc of Figure 6b and data [e.g., plate 2 of *Wright et al.*, 1999; Figure 2 of *Lyons et al.*, 2002].

[49] Observed large amplitude PSBL Alfvén waves have been shown to carry a current and Poynting vector sufficient to account for the electron energy flux into the ionosphere: In some events *Keiling et al.* [2002] found a significant fraction of the wave Poynting flux seen by Polar ($\sim$6 R_E)

was converted to electron energy flux into the ionosphere which then stimulated optical auroral emissions. In terms of our simulation, we could regard the earthward propagating wave as an "incident" wave which loses energy in the near-Earth region through energizing electrons. Hence any Alfvén wave reflected back to the tail would be expected to have a smaller amplitude than the incident wave. This suggests that Polar would observe a predominantly earthward propagating wave on PSBL field lines. In contrast, on lobe field lines we expect smaller Alfvén wave amplitudes and (coupled with weaker phasemixing) smaller $j_{\|}$.

[50] Consequently Alfvén waves on lobe field lines will only weakly energize electrons, and we expect the incident wave to be efficiently reflected from the near-Earth region. This will lead to a superposition of earthward (incident) and anti-earthward (reflected) waves. As seen in the simulations of *Allan and Wright* [2000] this combination gives the polarization of a local standing wave, as also seen in data recorded in the lobe [*Keiling et al.*, 2005]. In contrast, the smaller reflection coefficient appropriate for PSBL field lines suggest a mixed polarization somewhere between a standing wave and an earthward propagating wave is likely, and is also in accord with Keiling et al.'s observations.

[51] Our simulations do not model the propagation of the waves through the dipolar field geometry and down to the ionosphere, which leads to current intensification and electron acceleration. The link between a high altitude Poynting vector, electron precipitation and auroral luminosity is well-established in the observations cited above, however to model this requires at least a two-fluid description. Thus the present study is appropriate for focusing on the coupling of fast and Alfvén waves in the tail (where wave structures exceed kinetic and inertial scales). The inclusion of inertial effects in the dipolar region can lead to the development of parallel electric fields of the order of 1 mVm^{-1} [e.g., *Wright et al.*, 2002, and references therein].

5. Comparison With Observations

5.1. MSP Data

[52] As noted in section 4, mapping the PSBL simulation fields conservatively to the ionosphere can produce current densities of several μAm^{-2}. The ionospheric latitudinal scale can be estimated by reducing the z scale length of the simulation fields by a factor Z_{sc} = 40. This means a z interval of 0.1 in Figures 6 and 7 (which corresponds to 2.5 R_E in the tail) maps to 400 km (3.6° of latitude) in the ionosphere.

[53] The north-south extent of the >0.5 μAm^{-2} electron precipitation for the even modes (Figure 6), when mapped to the ionosphere corresponds to 40–80 km, and is similar for the odd modes in Figure 7 (35–130 km). This compares favorably with the data reported by *Wright et al.* [1999] (120–200 km) and *Lyons et al.* [2002] (60–200 km) given the crude mapping we employ.

[54] Recalling our normalizing time unit is 227.5 s, the period of the arcs produced by even modes (Figure 6) is 4.5–6 min. This is also similar to the higher harmonic arcs associated with odd modes (Figure 7b). The longest periods result from the fundamental odd mode and vary with driving parameters and location in the PSBL. They are typically 10–15 min, but the longest exceed 20 min. These agree well with the periods reported by *Wright et al.* [1999] of 5.4, 9.8, 16.7 and 18.5 min, and those of *Lyons et al.* [2002] (13–15 min and 25–30 min).

[55] The phase speeds in the ionosphere of the arcs in Figure 6 range from 0.28 to 0.72 kms^{-1}, while those in Figure 7 span 0.17 to 0.4 kms^{-1}. These compare well with the observations by *Wright et al.* [1999] of 0.34–0.76 kms^{-1}, and 0.5–1.0 kms^{-1} (estimated from Figure 2 of *Lyons et al.* [2002]).

5.2. Satellite Data

[56] The large amplitude ULF Alfvén waves seen by Polar at ~6 R_E have magnetic and electric field amplitudes of 2–20 nT and 10–80 Vm^{-1} [*Keiling et al.*, 2002, 2005]. They also showed that the ratio of E_z/b_y was similar to the Alfvén speed at Polar, supporting the interpretation of a propagating wave with an earthward Poynting vector. The background magnetic field at Polar was B_{Pol} ~400 nT, so there has been considerable convergence of the magnetic field from the tail (where B_T ~10 nT).

[57] A simple way of mapping our simulation wavefields from the tail to Polar is to assume that all the Alfvén wave energy reaches Polar. Conservation of energy transport along a flux tube requires that the product of Poynting vector and tube cross-section remains constant along the tube (i.e., $E_z b_y \times \text{Area} \propto E_z b_y/B = \text{const.}$). For a propagating Alfvén wave with $E_z = -V_A\, b_y$, where $V_A = B/\sqrt{\mu_0\rho}$, this means b_y and E_z will scale as

$$b_y \propto \rho^{\frac{1}{4}} \tag{13}$$

$$E_z \propto \frac{B}{\rho^{\frac{1}{4}}} \tag{14}$$

[58] The tail simulation was driven with a velocity amplitude of 320 kmp^{-1} in a tail of Alfvén speed V_{AT} = 700 kms^{-1} and field strength B_T = 10 nT. Thus the normalized b_y of 0.4 in Figures 4 and 5 corresponds to a dimensional value of ~2 nT. The Alfvén wave magnetic field amplitudes (not shown) for the simulations summarized in Figures 6 and 7 were a little larger, having dimensional values of between 4 and 9 nT. The electric field associated with a tail b_y of 2–9 nT is 1.4–6.3 mVm^{-1}.

[59] To map the Alfvén wavefields from the tail to Polar using (13, 14) we need to estimate the change in B (B_{Pol}/B_T = 400 nT/10 nT) and density. The latter can be deduced from

$$\left(\frac{\rho_{Pol}}{\rho_T}\right)^{\frac{1}{4}} = \left(\frac{B_{Pol}}{B_T}\cdot\frac{V_{AT}}{V_{APol}}\right)^{\frac{1}{2}} = 1.7 \tag{15}$$

where we have assumed V_{APol} = 10,000 kms^{-1} [see *Keiling et al.*, 2002]. Thus the tail magnetic field amplitudes of 2–9 nT will increase modestly to 3-15 nT at Polar, while the electric field amplitude of 1.4–6.3 mVm^{-1} will increase dramatically (by a factor of 24) to 30–150 mVm^{-1}. These agree well with the range of values reported by *Keiling et al.* [2002, 2005].

[60] Observations show that the Alfvén wave magnetic field is larger in the PSBL than in the lobe [*Wygant et al.*, 2000; *Keiling et al.*, 2002], and that the Poynting vector in

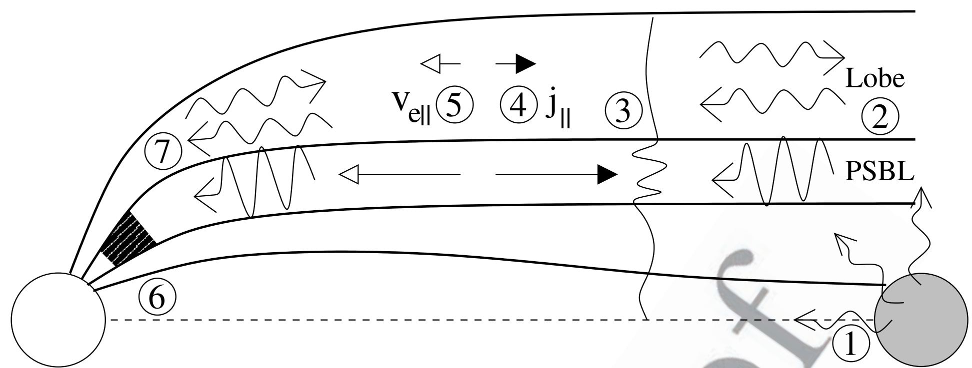

Figure 8. Sketch of coupling of energy release in the magnetotail to auroral arcs. (1) Energy release in the plasma sheet excites fast waveguide modes in the magnetotail. (2) The fast waves couple to Alfvén waves in the PSBL and lobe which propagate earthward. (3) The Alfvén waves phasemix as they propagate, leading to rapid variation of the wavefields perpendicular to **B** in the PSBL. (4) The Alfvén waves carry a field aligned current ($j_{||}$) which is strongest in the PSBL. (5) The $j_{||}$ is carried by electrons moving parallel to **B**. In the PSBL the electrons need to move with energies of around a keV, and are therefore capable of exciting optical auroral emissions (6) when they reach the ionosphere. (7) The electron acceleration on PSBL field lines depletes the Alfvén wave energy so there is little reflected (anti-earthward) component, in contrast to the lobe, where a strong reflected wave combines with the incident wave to give a local standing wave.

the PSBL exceeds that in the lobe by 2–3 orders of magnitude [*Keiling et al.*, 2005].

[61] Our simulations (see Figure 4) suggest that the waves will need to have a dawn-dusk wave number of $k_y \approx 7.5$ (dimensional half-wavelength of 10 R_E), and give b_y(PSBL) exceeding b_y(lobe) by a factor of 20. The ratio of the Poynting vector in the PSBL and lobe may be expressed as

$$\frac{(b_y u_y B_0/\mu_0)_{\mathrm{PSBL}}}{(b_y u_y B_0/\mu_o)_{\mathrm{lobe}}} \equiv \frac{\left(b_y^2 V_A\right)_{\mathrm{PSBL}}}{\left(b_y^2 V_A\right)_{\mathrm{lobe}}} \tag{16}$$

[62] Given that $u_y B_0 = \pm b_y V_A$, and that V_A in the center of the PSBL is about 0.5 of that in the lobe (Figure 1), the Poynting vector ratio is $\sim$200, in accord with the estimates of *Keiling et al.* [2005]. Note that these observations were recorded by Polar at $\sim$6 R_E. It is to be expected that mapping the Poynting vector from the tail to 6 R_E will increase its magnitude. However, since this increase will be similar for adjacent lobe and PSBL field lines, we expect the ratio in (16) to be similar to that seen by Polar.

[63] The scenario we advocate assumes that the larger Poynting vector in the PSBL is necessary to accelerate electrons to carry the intense $j_{||}$ that exists there. As these electrons precipitate and produce auroral intensification, it provides a natural explanation for the correlation of Poynting vector with auroral intensity [*Wygant et al.*, 2000; *Keiling et al.*, 2002] and hence energy of precipitating electrons. The significant conversion of Poynting flux associated with the earthward propagating PSBL Alfvén wave to electron energy flux leads to the absence of a strong reflected wave from the near-Earth region, in contrast to the behavior on lobe field lines where the superposition of waves gives a standing wave polarization. These features are seen in the spacecraft data reported by *Keiling et al.* [2005]. The relation between upward current, Poynting vector, and auroral intensity established in data has been exploited to allow us to relate the upward current contours from the tail in Figures 6 and 7 to auroral arc intensity data.

6. Summary

[64] In this paper we have performed numerical simulations of MHD wave coupling in a magnetotail waveguide. The simulation itself is quite simple and idealized, but when augmented by features established by other studies, forms the center of a description that provides a coherent view of many details of ULF Alfvén waves in the magnetotail. The extended scenario that emerges is shown schematically in Figure 8.

[65] (1) Energy release in the tail such as from substorms can release fast mode energy into the magnetotail waveguide.

[66] (2) Earthward of the site of energy release the fast modes couple to earthward propagating Alfvén waves. Those in the lobe travel the fastest, and their detection by satellites can be used as a new indicator of substorm onset (coincident with traditional signatures seen in ground magnetometer data) [*Keiling et al.*, 2005]. If the dawn-dusk extent of the energy release site is $\sim 10 R_E$, the PSBL Alfvén waves will have a much larger amplitude and Poynting vector than those in the lobe.

[67] (3) The nonuniform Alfvén speed in the tail refracts the Alfvén waves and they develop phase structure in the z direction through the process of phasemixing. This occurs most efficiently where dV_A/dz is largest. Hence the wavelength in z is much smaller in the PSBL than in the lobe.

[68] (4) The Alfvén wave $j_{||}$ is proportional to the wave's b_y amplitude divided by the wavelength in the z direction. Both of these factors contribute to $j_{||}$ in the PSBL far exceeding that in the lobe.

[69] (5) $j_{||}$ is carried predominantly by electrons traveling along field lines. The speed of electrons in the PSBL, and

hence the energy transferred to them from the Alfvén wave, is greater than that in the lobe. This behavior is enhanced as the current flow approaches the earth, where the converging field geometry intensifies $j_{||}$ further.

[70] (6) The downgoing electrons precipitate in the ionosphere. On PSBL field lines $j_{||}$ can reach several μAm^{-2}, requiring electrons to have energies of several keV [e.g., *Lotko et al.*, 1998]. Much lower energies are expected on lobe field lines. PSBL precipitating electrons will have sufficient energy to produce optical auroral emissions [e.g., *Wright et al.*, 1999; *Samson et al.*, 2003], while those on lobe field lines will generally not. The phase motion of the arcs on PSBL field lines will be the same as that of the Alfvén wave; namely, equatorward with speeds of about 1 kms^{-1}.

[71] (7) The energy given by PSBL Alfvén waves to electrons may be so significant that there is little or no reflected wave here from the near Earth and ionospheric environment. This means PSBL waves will favor the polarization of earthward propagating waves, with a Poynting vector directed earthward. In contrast, lobe Alfvén waves lose little energy to electrons and may undergo efficient reflection from the ionosphere. This will result in a superposition of earthward and anti-earthward propagating Alfvén waves in the lobe, which will have a polarization similar to a standing Alfvén wave and a Poynting vector whose direction alternates throughout a wave cycle.

[72] **Acknowledgments.** The authors are grateful to Andreas Keiling and Larry Lyons for helpful discussions.

[73] Amitava Bhattacharjee thanks the reviewers for their assistance in evaluating this paper.

References

Allan, W., and F. B. Knox (1979), A dipole field model for axisymmetric Alfvén waves with finite ionosphere conductivities, *Planet. Space Sci.*, *27*, 79.

Allan, W., and A. N. Wright (1998), Hydromagnetic wave propagation and coupling in a magnetotail waveguide, *J. Geophys. Res.*, *103*, 2359.

Allan, W., and A. N. Wright (2000), Magnetotail waveguide: Fast and Alfvén waves in the plasma sheet boundary layer and lobe, *J. Geophys. Res*, *105*, 317.

Allan, W., S. P. White, and E. M. Poulter (1986), Impulse-excited hydromagnetic cavity and field-line resonances in the magnetosphere, *Planet. Space Sci.*, *34*, 371.

Chen, L., and A. Hasegawa (1974), A theory of long-period magnetic pulsations, 1, Steady state excitation of field line resonance, *J. Geophys. Res.*, *79*, 1024.

Dombeck, J., C. Cattell, J. R. Wygant, A. Keiling, and J. Scudder (2005), Alfvén waves and Poynting flux observed simultaneously by Polar and FAST in the plasma sheet boundary layer, *J. Geophys. Res.*, *110*, A12S90, doi:10.1029/2005JA011269.

Edwin, P. M., B. Roberts, and W. J. Hughes (1986), Dispersive ducting of MHD waves in the plasma sheet: A source of Pi2 wave bursts, *Geophys. Res. Lett.*, *13*, 373.

Herron, T. J. (1967), An average geomagnetic power spectrum for the period range 4.5 to 12900 seconds, *J. Geophys. Res.*, *72*, 759–761.

Hopcraft, K. I., and P. R. Smith (1986), Magnetohydrodynamic waves in a neutral sheet, *Planet. Space Sci.*, *34*, 1253.

Keiling, A., J. R. Wygant, C. Cattell, W. Peria, G. Parks, M. Temerin, F. S. Moser, C. T. Russell, and C. A. Kletzing (2002), Correlation of Alfvén wave Poynting flux in the plasma sheet at 4–7 RE with ionospheric electron energy flux, *J. Geophys. Res.*, *107*(A7), 1132, doi:10.1029/2001JA900140.

Keiling, A., et al. (2005), Some properties of Alfvén waves: Observations in the tail lobes and plasma sheet boundary layer, *J. Geophys. Res.*, *110*, A10S11, doi:10.1029/2004JA010907.

Kivelson, M. G., and D. J. Southwood (1986), Coupling of global magnetospheric MHD eigenmodes to field line resonances, *J. Geophys. Res.*, *91*, 4345.

Lee, D. H., and R. L. Lysak (1989), Magnetospheric ULF wave coupling in the dipole model: the impulsive excitation, *J. Geophys. Res.*, *94*, 17,097.

Liu, W. W., B.-L. Xu, J. C. Samson, and G. Rostoker (1995), Theory and observations of auroral substorms: A magnetohydrodynamic approach, *J. Geophys. Res.*, *100*, 79.

Lotko, W., A. V. Streltsov, and C. W. Carlson (1998), Discrete auroral arc, electrostatic shock and suprathermal electrons powered by dispersive, anomalously resistive field line resonance, *Geophys. Res. Lett.*, *25*, 4449.

Lyons, L. R., et al. (2002), Auroral poleward boundary intensifications and tail bursty flows: A manifestation of a large-scale ULF oscillation?, *J. Geophys. Res.*, *107*(A11), 1352, doi:10.1029/2001JA000242.

Mann, I. R., A. N. Wright, and P. S. Cally (1995), Coupling of magnetospheric cavity modes to field line resonances: A study of resonance widths, *J. Geophys. Res.*, *100*, 19,441.

McClay, J. F., and H. R. Radoski (1967), Hydromagnetic propagation in a theta-model geomagnetic tail, *J. Geophys. Res.*, *72*, 4525.

Patel, V. L. (1968), Magnetospheric tail as a hydromagnetic waveguide, *Phys. Lett.*, *26A*, 596.

Ruderman, M. S., and B. Roberts (2002), The damping of coronal loop oscillations, *ApJ.*, *577*, 475.

Samson, J. C., L. L. Cogger, and Q. Pao (1996), Observations of field line resonances, auroral arcs, and auroral vortex structures, *J. Geophys. Res.*, *101*, 17,373.

Samson, J. C., R. Rankin, and V. T. Tikhonchuk (2003), Optical signatures of auroral arcs produced by field line resonances: Comparison with satellite observations and modeling, *Ann. Geophys.*, *21*, 933.

Southwood, D. J. (1974), Some features of field line resonances in the magnetosphere, *Planet. Space Sci.*, *22*, 483.

Vaivads, A., et al. (2003), What high altitude observations tell us about the auroral acceleration: A Cluster/DMSP conjunction, *Geophys. Res. Lett.*, *30*(3), 1106, doi:10.1029/2002GL016006.

Wright, A. N., and I. R. Mann (2007), Global MHD eigenmodes of the outer magnetosphere, AGU Monograph, in press.

Wright, A. N., and G. J. Rickard (1995), A numerical study of resonant absorption in a magnetohydrodynamic cavity driven by a broadband spectrum, *Astrophys. J.*, *444*, 458.

Wright, A. N., W. Allan, and P. A. Damiano (2003), Alfvén wave dissipation via electron energization, *Geophys. Res. Lett.*, *30*(16), 1847, doi:10.1029/2003GL017605.

Wright, A. N., W. Allan, R. D. Elphinstone, and L. L. Cogger (1999), Phasemixing and phase motion of Alfvén waves on tail-like and dipole-like magnetic field lines, *J. Geophys. Res*, *104*, 10,159.

Wright, A. N., W. Allan, M. R. Ruderman, and R. C. Elphic (2002), The dynamics of current carriers in standing Alfvén waves: Parallel electric fields in the auroral acceleration region, *J. Geophys. Res.*, *107*(A7), 1120, doi:10.1029/2001JA900168.

Wygant, et al. (2000), Polar spacecraft based comparison of intense electric fields and Poynting flux near and within the plasma sheet-tail lobe boundary to UVI images: An energy source for the aurora, *J. Geophys. Res.*, *105*, 18,675.

Xu, B.-L., J. C. Samson, W. W. Liu, F. Creutzberg, and T. J. Hughes (1993), Observations of optical aurora modulated by resonant Alfvén waves, *J. Geophys. Res.*, *98*, 11,531.

W. Allan, National Institute of Water and Atmospheric Research, P. O. Box 14-901, Kilbirnie, Wellington, New Zealand. (w.allan@niwa.cri.nz)

A. N. Wright, Mathematical Institute, University of St. Andrews, St. Andrews, Fife KY16 9SS, UK. (pdamiano@mcs.st-and.ac.uk; andy@mcs.st-and.ac.uk)

American Geophysical Union
Author Query Form

Journal: **Journal of Geophysical Research - Space Physics**
Article Name: Wright(2007JA012464)

Please answer all author queries.

1. Citation of Section 2.3.1 was changed to section 2.2.1. Please check if appropriate.

2. Figure 7b cited in the text but the corresponding figure caption has no (a) and (b) parts.